IEEE Access
Multidisciplinary | Rapid Review | Open Access Journal

Received August 4, 2020, accepted August 12, 2020, date of publication August 17, 2020, date of current version August 28, 2020.

Digital Object Identifier 10.1109/ACCESS.2020.3017195

Complementary Constrained Model Predictive Depth Control of a Hybridly-Actuated Submarine Drifter

DALEI SONG[1,2], RENYU HOU[1], CHONG LI[1], JOHN Y. HUNG[3], AND JILIANG WANG[3], (Graduate Student Member, IEEE)

[1]School of Engineering, Ocean University of China, Qingdao 266100, China
[2]Institute for Advanced Ocean Study, Ocean University of China, Qingdao 266100, China
[3]Department of Electrical and Computer Engineering, Auburn University, Auburn, AL 36849, USA

Corresponding author: Chong Li (czl0047@auburn.edu)

This work was supported in part by the Fundamental Research Funds for the Central Universities under Grant 201962012, in part by the National Natural Science Foundation of China under Grant 41527901, and in part by the Aoshan Innovation Program of Pilot National Laboratory for Marine Science and Technology of Qingdao under Grant 2017ASKJ01.

ABSTRACT The submarine drifter is a novel Lagrangian-based observation platform to explore the ocean, but its precise and rapid depth control system design is still an open issue. The major challenge would be the complex hybrid actuation system, which contains anisotropic characteristics and switching issues. In this paper, we proposed an modified complementary constrained model predictive control (MCC-MPC) scheme to meet the metrics. The scheme reformulates complex drifter and hybrid actuation system dynamics into a solvable system with complementary constraints. The nonlinear component inside the system is approximated by applying a sgn-sigmoid approximation function for the sake of linearization and computation. Then the customized online optimizer predicts the system dynamics with complementary constraints and computes the optimal control outputs in the finite horizon in an iterative loop. The validation results prove that the proposed controller can effectively control the submarine drifter to achieve the desired depth and the key metrics are 10x, 4x, and 2x better than conventional PID control, disturbance observer-based control, and conventional MPC methods, respectively.

INDEX TERMS Submarine drifter, hybrid actuation system, complementary constraints, model predictive control.

I. INTRODUCTION

Ocean observation technology is a crucial topic since it's essential to protect the ocean environment, mine ocean resources, and prevent ocean hazards. The observation methods can be divided into space-based and sea-based: space-based observations use satellite remote sensing technology or aircraft to obtain sea surface remote sensing data; sea-based observations are referred to the measurement systems deployed on vessels, which is the most direct and reliable way to observe ocean. The commonly used ocean mobile observation platforms including ocean research ships, ocean observation stations, and unmanned ocean mobile observation platforms provide more detailed observations of the ocean. In recent years, with the rise of intelligent technology, unmanned ocean mobile observation platforms (e.g., Argo, autonomous underwater vehicle (AUV), underwater glider, unmanned vessel, drifter, etc.) carrying variety of sensors can perform a series of important tasks in the extreme ocean environment. Though there are still lots of problems of these intelligent platforms, especially, if the observation problem is unique. The ocean current observation is an attractive area for scientists, but the existing methods do not meet the desired performance metrics yet. Argos are challenging to meet precise depth control requirements to conduct reliable measurement because of its inherent driving systems [1]. Their depth is adjusted by a mechanism of a plunger pump to change its gravity which is sensitive to the sea density. Underwater gliders are designed with better driving systems but they do not fit the fine-scale measurement tasks [2], [3]. AUVs that utilize propellers can provide precise position control and are considered as ideal platforms for ocean observation [4], [5]. But its propellers can significantly affect the nature of the ocean current. Unmanned vessels [6] can replace traditional ocean research ship with Acoustic Doppler Current Profiler (ADCP) [7] to fulfill a part of the tasks, but the measurement

The associate editor coordinating the review of this manuscript and approving it for publication was Ton Duc Do.

ranges are limited to the sea surface while three-dimensional information is incomplete.

As a Lagrangian-based observation method, the drifter requires the observation platform to follow the current effectively and can intuitively reflect some physical phenomena in the ocean [8]. Therefore, it can be used for a fine-scale observation of the ocean to make up for the shortcomings of other observation methods [9] (e.g., fixed-point Euler observation using ADCP, self-propelled observation using AUV, glider and vessel, etc.). For example, [10] reveal the influence of geostrophic strain on oceanic ageostrophic motion and surface chlorophyll using the surface drifter; [11] use the drifter to observe submesoscale flow kinematics in the coastal ocean, etc. However, the existing drifters only can follow the two-dimensional flow at the ocean surface or near surface because of their positive buoyancy. Although floats like Argo can change their gravity to dive, they do not have the function of following the current effectively and their depth control is not precise, so they cannot be used as drifter for three-dimensional observation. It's the lack of observation techniques including underwater depth control of the drifter that hinders the application of three-dimensional Lagrangian observation and scientists' further studying of the ocean [12]–[14].

At present, the research works of depth control for underwater vessels are mainly focused on AUVs and remotely operated vehicles (ROVs). For example, [15] use gain-scheduled reduced order output feedback and [16] use reinforcement learning to achieve the depth control of AUVs; [17] use fuzzy PID and [18] use neural network predictive control to provide solutions for the depth control of ROVs. The optimized finite time stabilized attitude control approach with fault-tolerant capability can be also adapted to ROVs and other under water vessels [19], [20]. However, there is no ideal solution to the depth control problem of the drifter. It can't install propellers to reformulate the control problems to AUVs, etc. Because these active driving systems disturb the surrounding flow field and lead the observation tasks to be failed.

By investigating the principles of the different platforms, we propose a novel oceanic observation platform namely submarine drifter with both current following and precision depth control capability. The idea is originated from Argo and surface drifter, but the mechanical structures and the driving systems are completely redesigned. As shown in Fig. 1, the drifter is equipped with sails to improve its ability to follow the current, and hybrid driving system which will be discussed in detail in the next section is used as an actuator for the depth control. Although this design can effectively solve the hardware problem in the application, hybrid driving system greatly increases the difficulty of the control system.

The hybrid depth actuation system is composed of a gear pump and a solenoid valve, which makes the ascending and diving control anisotropic (asymmetrical). Classical solutions like PID control calculate the control output through feedback results without considering these problems, which will cause

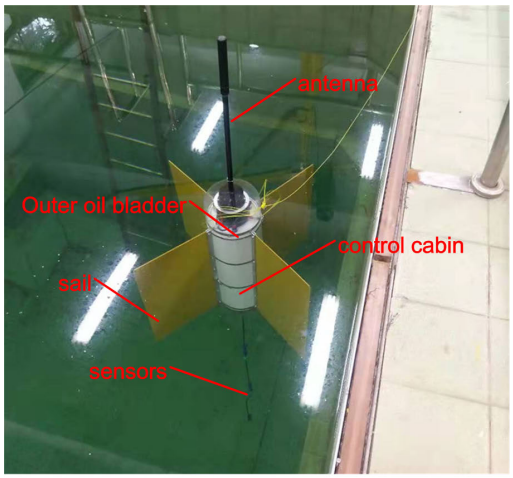

(a) Submarine drifter in indoor pool environment.

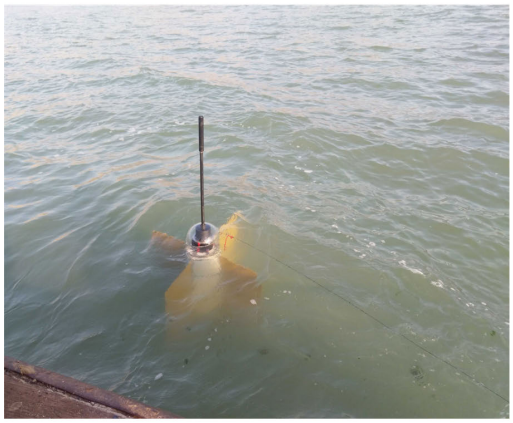

(b) Submarine drifter in ocean environment.

FIGURE 1. The actual submarine drifter in different environments.

the driving system to switch passively between the pump and the valve in order to track the control output. Thus, a good performance of depth control cannot be guaranteed. For the ascending and diving directions, the system shows anisotropic characteristics which can be usually formulated as switched control problems. Due to the theoretical difficulties, the authors are proposing an alternative approach. MPC is a kind of optimal control, which can transform nonlinear control problem of the drifter into real-time linear optimal control problem with constraints and be solved by linear quadratic programming [21]. It has the potential to provide the rapidly and precise depth control function for the drifter, if two barriers can be overcome: (1) computation costs and (2) hybrid driving system formulation. The underwater motion of submarine drifter has the characteristics of low dynamic ranges and the macro actuator is not designed to switch rapidly, so the overall bandwidth of the drifter is low enough to allow the engineering to implement complex depth control algorithms of the drifter. The hybrid driving system is also modeled as two actuators with complementary constraints, so the MPC frameworks can be valid.

The main contributions of this paper can be summarized as follows:

(1) The intrinsic dynamics of the submarine drifter is analyzed. The unique time delay mechanism and hybrid actuation system inside the drifter are modeled and further approximated for engineering practice.

(2) Modified complementary constrained model predictive control (MCCMPC) is proposed for the depth control, which can handle the nonlinear switching and time delay characteristics with improved settling time and steady state performance.

(3) The computational costs are analyzed and optimized with a customized online solver. This solver transforms the nonlinear optimization problem into an equivalent linear system to accelerate the computation process.

(4) The performance and advantage of the proposed method have been verified with the comparison of other potential controllers. The results show that MCCMPC can effectively control the drifter to the desired depth set point and the key metrics are significantly better than PID control, disturbance observer based control, and conventional model predictive control (MPC).

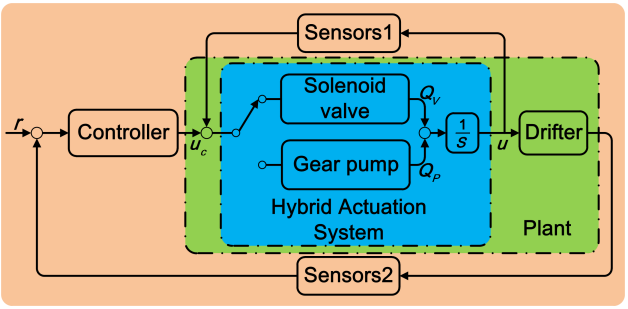

FIGURE 2. The control scheme of submarine drifter.

II. SUBMARINE DRIFTER MODEL

A. BOUYANCY MECHANISM

Bouyancy is changed by varying the displacement of the drifter, through an oil-filled bladder system. The control scheme and the inner dynamics of submarine drifter are shown in Fig. 2. The hybrid actuation system (in the blue box) consists of the pump and the valve, which are used to vary the bladder volume. The challenge is that these two mechanisms have completely different dynamic characteristics, and their relationship with the controller is like a single-pole double-throw switch, which will cause discontinuity and anisotropy in modeling and step-like jumps in control. To establish a feasible control solution, these switching dynamics must be investigated and modeled in a practical way. The reminder of this section gives these details.

B. DYNAMIC ANALYSIS

By design, the drifter center of gravity is far lower than its center of buoyancy. Consequently, the submerged drifter maintains a vertical, upright orientation. Define d to be the drifter depth. The vertical motion dynamic is described by:

$$m\ddot{d} + k\dot{d}^2 \operatorname{sgn}(\dot{d}) = F, \tag{1}$$

where m is the drifter mass, k is the water damping coefficient, $\operatorname{sgn}(\cdot)$ is the signum (sign) function, and F is net buoyancy of the drifter. Net bouyancy is modeled as:

$$F = G - F_b, \tag{2}$$

where G is the drifter weight, and F_b is the *controlled* buoyancy that is changed by the bladder volume. At equilibrium, $F = 0$, velocity $\dot{d} = 0$, and the drifter is suspended in the water.

The relationship between actuator output u and controlled buoyancy F_b is given by:

$$F_b = k_{uF} \cdot u, \tag{3}$$

where k_{uF} is a buoyancy conversion coefficient for the actuator output u. The hybrid actuation system is furthered described next.

C. HYBRID ACTUATION SYSTEM

As shown in Fig. 3(a), the drifer's hybrid actuation system is mainly composed of a outer oil bladder, gear pump, solenoid valve and inner oil bladder. The outer oil bladder is outside of the control cabin and bears the water pressure, while the other components of the system are installed inside the fixed-volume control cabin. Because the reverse pressure capacity of the pump is low, a one-way check valve is in series with the pump. Otherwise, hydraulic oil will leak back into the inner oil bladder from the outer oil bladder when the reverse pressure is high. The other control branch consists of a solenoid valve. By controlling the flow of hydraulic oil between oil bladders, the system can change the volume of the outer oil bladder, and thusly control buoyancy F_b of the drifter.

When the gear pump is turned on and the solenoid valve is closed, the hybrid actuation system is equivalent to the situation shown in Fig. 3(b). The hydraulic oil is discharged from the inner oil bladder to the outer oil bladder under the action of the pump, and buoyancy increases.

When the solenoid valve is turned on and the gear pump is closed, the hybrid actuation system is equivalent to the situation shown in Fig. 3(c). Water pressure forces hydraulic oil back into the inner oil bladder, reducing the volume of the outer bladder, resulting in decrease of bouyancy.

The pump and the valve can not be simultaneously opened; the actuator is either in the mode of Fig. 3(b) or Fig. 3(c).

D. MODELING WITH COMPLEMENTARY CONSTRAINTS

The drifter's ascent and descent dynamics are dfferent, and there are step-like jumps in the control because of the switching actions of pump and solenoid valve. In this work, two complementary constraints apply to the hybrid actuation system:

$$Q = Q_V + Q_P \;\; Q_V \cdot Q_P = 0, \tag{4}$$

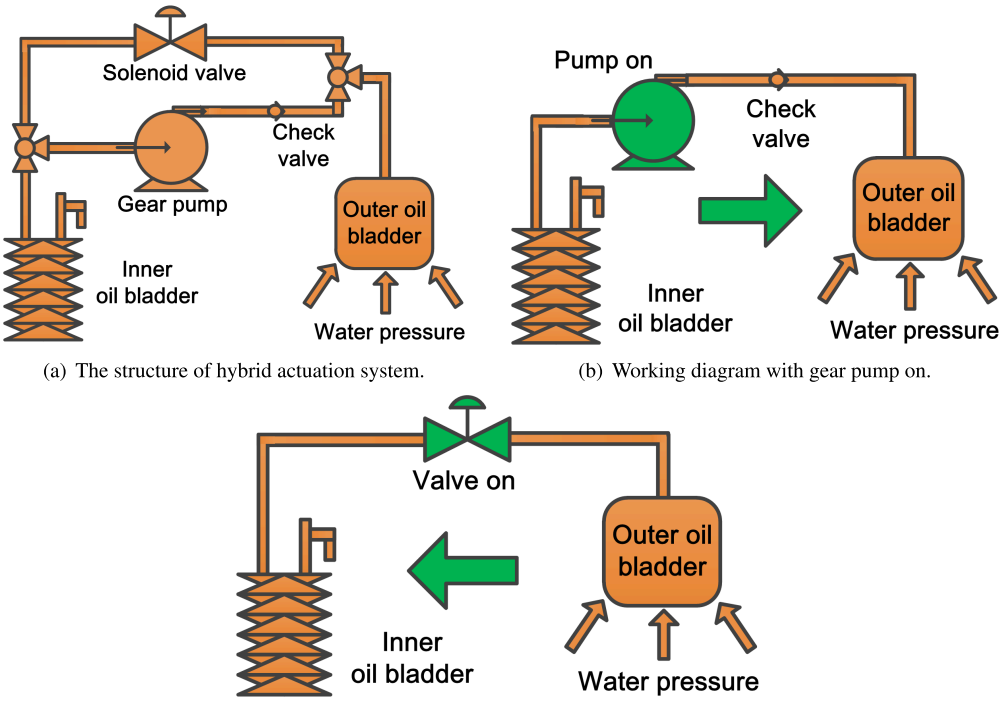

(a) The structure of hybrid actuation system.

(b) Working diagram with gear pump on.

(c) Working diagram with solenoid valve on.

FIGURE 3. (a) Shows the structure of the hybrid actuation system, and (b) (c) show its equivalent structure under different working conditions.

where Q is the hybrid actuation system flow rate, Q_V is the solenoid valve flow rate, and Q_P is the pump flow rate. Valve and pump flow rates are modeled as:

$$\begin{aligned} Q_V &= \max[0, \operatorname{sgn}(u_c - u)] \cdot f(\Delta p) \\ Q_P &= \max[0, \operatorname{sgn}(u - u_c)] \cdot k_p, \end{aligned} \tag{5}$$

where u_c is the output of controller, k_p is the flow rate coefficient of pump, and $f(\Delta p)$ is the flow rate coefficient of solenoid valve. Coefficient $f(\Delta p)$ is a function of the differential pressure Δp across the valve, and is modeled by:

$$f(\Delta p) = k_{pq}\sqrt{k_{dp}d + p_{atmos} - p_{in}}, \tag{6}$$

where k_{pq} is the pressure-flow (p, q) conversion coefficient, k_{dp} is the depth-pressure (d, p) conversion coefficient, d is drifter depth as explained earlier, p_{atmos} is atmospheric pressure, and p_{in} is the inner oil bladder pressure.

Analysis of (5) and (6) shows that drifter depth affects the solenoid valve flow rate in nonlinear manner, but the pump flow rate is a constant value. When the drifter is at the water surface, k_p is about eight times larger than $f(\Delta p)$. As such, there is a significant nonlinear difference in flow characteristics between the pump and the valve.

Define the state vector $\boldsymbol{x}$ with variables $x_1 = d$, $x_2 = \dot{d}$, $x_3 = u$. Then the state space model of submarine drifter dynamics takes the form:

$$\dot{\boldsymbol{x}} = \boldsymbol{f}(\boldsymbol{x}, u_c), \tag{7}$$

where $\boldsymbol{x} \in \mathrm{R}^3$, $u_c \in \mathrm{R}$, and vector field $\boldsymbol{f}$ is given by:

$$\boldsymbol{f}(\boldsymbol{x}, u_c) = \begin{pmatrix} x_2 \\ (k_{uF}x_3 - k{x_2}^2 \operatorname{sgn}(x_2))/m \\ \max[0, \operatorname{sgn}(u_c - x_3)] \cdot f(\Delta p) + \\ \max[0, \operatorname{sgn}(x_3 - u_c)] \cdot k_p \end{pmatrix}. \tag{8}$$

Because of the particular design structure of hybrid actuation system, the buoyancy control has to switch between the pump and the valve with distinct difference in flow characteristics. Moreover, it needs time for the actuator to track the control output, which leads to different control response delays under the action of the pump or the valve.

Classical solution approaches like PID control do not directly consider these problems, so a small settling time with response that is free of oscillations cannot be guaranteed. For the ascending and diving directions, the system shows anisotropic characteristics that can be usually formulated as switched control problems. In view of these theoretical difficulties, an alternative approach based on model predictive control (MPC) is used in this work.

MPC has the potential to provide the rapid, precise depth control function for the drifter, if two barriers can be overcome: (1) large computation time, and (2) hybrid driving system formulation. The hybrid actuator is not designed to switch rapidly, however, and the overall bandwidth of the drifter is low enough to allow implementation of complex depth control algorithms. The hybrid driving system is also modeled as two actuators with complementary constraints, so an MPC-based framework is suitable.

In the next section, a conventional MPC approach and its shortcomings are briefly described, followed by description of the main contribution, which is a modified complementary constrained MPC, hereafter abbreviated as MCCMPC.

III. PROPOSED CONTROL STRATEGY

Conventional MPC for drifter depth control is discussed in the first subsection for sake of providing prerequisite materials for the proposed control method. The second subsection details the MPC strategy with MCCMPC.

A. CONVENTIONAL MPC

There are two different approaches to implement model prediction. The first approach is that the anisotropy of model (8) can be considered as one of two separate cases:

If $u_c \geq x_3$, then the solenoid valve will be opened and the following equivalent submodel is used for MPC prediction,

$$\boldsymbol{f}(\boldsymbol{x}, u_c) = \begin{pmatrix} x_2 \\ (k_{uF} x_3 - k x_2^2 \operatorname{sgn}(x_2))/m \\ f(\Delta p) \end{pmatrix}. \tag{9}$$

Otherwise, $u_c < x_3$, the gear pump will be turned on, and the following submodel will be used,

$$\boldsymbol{f}(\boldsymbol{x}, u_c) = \begin{pmatrix} x_2 \\ (k_{uF} x_3 - k x_2^2 \operatorname{sgn}(x_2))/m \\ k_p \end{pmatrix}. \tag{10}$$

This first approach does not solve the discontinuity of model (8). Discontinuous switching between two prediction submodels will occur, which can lead to control extremes (overly timid or overly strong).

A second approach is to avoid switching between prediction submodels (9) and (10). A fixed prediction model could be based on the submodel with smaller gain, i.e. use the submodel that is more conservative. This approach solves the problem of discontinuity, but sacrifices prediction accuracy.

B. MPC WITH MODIFIED COMPLEMENTARY CONSTRAINTS

To overcome the above barriers and drawbacks, a MCCMPC approach that fully considers the anisotropy and discontinuity of the drifter dynamics is presented here.

1) MODEL PREPROCESSING

The complex actual model behavior is the first barrier to be removed, by using several model preprocessing actions. Firstly, the original complex single-input, single-output system with max function is converted to a two-input, single-output system. Next, each discontinuous sgn function in the system model is replaced by a smooth approximation. Lastly, linearization is applied.

In model (8), the control u_c is either the solenoid valve control value u_v, or the gear pump control value u_p. Therefore, the max function can be eliminated by introducing a complementary equality constraint:

$$(u_v - x_3)(u_p - x_3) = 0. \tag{11}$$

The physical principles of the hybrid actuation system are reflected by additional inequality constraints:

$$x_3 \leq u_v \leq u_{max} \quad \text{and} \quad u_{min} \leq u_p \leq x_3 \tag{12}$$

where u_{max}, u_{min} are the respective maximum and minimum output of hybrid actuation system. These equations show that the boundary of constraints is dynamic and the optimal solution must satisfy one-way flows of the pump and valve. Therefore, equations (4), (5) are equivalent to these relations:

$$\begin{aligned} Q &= \operatorname{sgn}(u_v - x_3) f(\Delta p) + \operatorname{sgn}(x_3 - u_p) k_p \\ x_3 &\leq u_v \leq u_{max} \\ u_{min} &\leq u_p \leq x_3 \\ (u_v - x_3)(u_p - x_3) &= 0 \end{aligned} \tag{13}$$

The sgn function is next approximated by a sigmoid function:

$$S(x) = \frac{2}{1 + e^{-k_s x}} - 1, \tag{14}$$

where $k_s \geq 0$ is the sigmoid coefficient that affects approximation accuracy. Fig. 4 shows a comparison of the sgn and $S(x)$ curves for $k_s = 1, 10$, and 100. Choosing a large k_s makes the $S(x)$ curve very similar to the sgn function, but also causes the sigmoid to be insensitive to the argument x, and affects the numerical stability of the optimization solver.

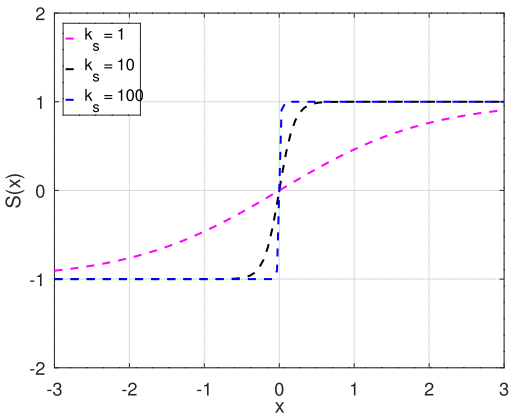

FIGURE 4. Three sigmoid functions $S(x)$, for $k_s = 1, 10, 100$.

To illustrate the feasibility of approximating the sgn function, the original model (8) is compared to one having the approximation $S(x)$ with $k_s = 100$. Three different input signals (unit step, unit pulse train, and unit sine) are used to excite the two models. The frequency of pulse train and sine wave is 0.5 Hz, and the initial depth $d = 10$ m. The results are shown in Fig. 5. With the step signal, the valve remains open and the drifter descends (dives). Under the action of periodic signals, the pump and the valve switch at a frequency of 0.5 Hz and because $Q_P > Q_V$, the drifter ascends (decreasing depth). Original and approximate models exhibit almost no differences in response to these typical signals.

After conversion and approximation of the system model, the state-space model of the drifter dynamics with two inputs

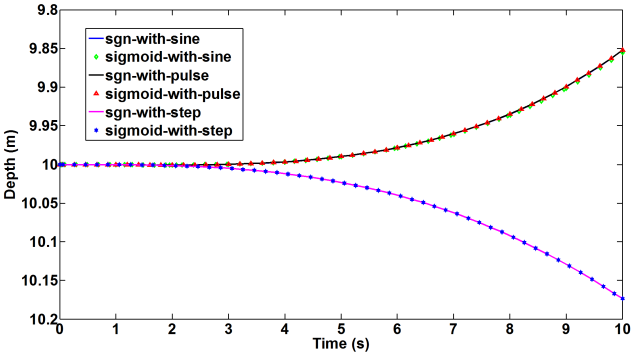

FIGURE 5. Comparison of response to different excitation signal between *sign* and *sigmoid* when $k_s = 100$.

becomes:

$$\begin{bmatrix} \dot{x}_1 \\ \dot{x}_2 \\ \dot{x}_3 \end{bmatrix} = \begin{bmatrix} x_2 \\ (k_{uF}x_3 - k \cdot {x_2}^2 S(x_2))/m \\ S(u_v - x_3)f(\Delta p) + S(x_3 - u_p)k_p \end{bmatrix}.$$
$$x_3 \le u_v \le u_{max}$$
$$u_{min} \le u_p \le x_3$$
$$(u_v - x_3)(u_p - x_3) = 0 \tag{15}$$

The final step of model preprocessing is linearization of (15), which is performed in every MPC iteration. The linearized model takes the form:

$$\dot{\boldsymbol{x}} = \boldsymbol{A}_c\boldsymbol{x} + \boldsymbol{B}_c\boldsymbol{u}. \tag{16}$$

Note that the preprocessing results in a two-input model, where bold-face $\boldsymbol{u} \in \mathrm{R}^2$ is a vector with elements representing the valve and pump effects.

2) MCCMPC STRATEGY

For online numerical calculations, state-space model (16) is discretized:

$$\boldsymbol{x}_d(k+1) = \boldsymbol{A}_d\boldsymbol{x}_d(k) + \boldsymbol{B}_d\boldsymbol{u}(k), \quad y(k) = \boldsymbol{C}_d\boldsymbol{x}_d(k). \tag{17}$$

In the above, subscript d denotes discrete-time, and should not be confused with the symbol for water depth. To improve steady-state performance, integrating control action is introduced by rewriting model (17) in incremental form and augmenting the model as follows:

$$\overbrace{\begin{bmatrix} \boldsymbol{x}(k+1) \\ \Delta\boldsymbol{x}_d(k+1) \\ y(k+1) \end{bmatrix}}^{} = \overbrace{\begin{bmatrix} \boldsymbol{A}_d & \boldsymbol{O} \\ \boldsymbol{C}_d\boldsymbol{A}_d & 1 \end{bmatrix}}^{\boldsymbol{A}} \overbrace{\begin{bmatrix} \boldsymbol{x}(k) \\ \Delta\boldsymbol{x}_d(k) \\ y(k) \end{bmatrix}}^{} + \overbrace{\begin{bmatrix} \boldsymbol{B}_d \\ \boldsymbol{C}_d\boldsymbol{B}_d \end{bmatrix}}^{\boldsymbol{B}} \Delta\boldsymbol{u}(k)$$
$$y(k) = \overbrace{\begin{bmatrix} \boldsymbol{O}^T & 1 \end{bmatrix}}^{\boldsymbol{C}} \begin{bmatrix} \Delta\boldsymbol{x}_d(k) \\ y(k) \end{bmatrix}, \tag{18}$$

where $\boldsymbol{A} \in \mathrm{R}^{4\times4}, \boldsymbol{B} \in \mathrm{R}^{4\times2}, \boldsymbol{C} \in \mathrm{R}^{1\times4}, \boldsymbol{O} \in \mathrm{R}^{3\times1}, \Delta\boldsymbol{x}_d(k) = \boldsymbol{x}_d(k) - \boldsymbol{x}_d(k-1), \Delta\boldsymbol{u}(k) = \boldsymbol{u}(k) - \boldsymbol{u}(k-1)$.

Define the control sequence

$$\Delta\boldsymbol{U} = [\Delta\boldsymbol{u}(k)\ \Delta\boldsymbol{u}(k+1)\ \cdots\ \Delta\boldsymbol{u}(N_c-1)]^T,$$

where N_c is the control horizon, and define the output prediction sequence

$$\boldsymbol{Y} = [y(k+1|k)\ y(k+2|k)\ \cdots\ y(k+N_p|k)]^T,$$

where N_p is the prediction horizon. Here $\Delta\boldsymbol{u}(k)$ is the control increment at time k, and $y(k+1|k)$ is the output of the time $k+1$ predicted at time k. The relationship between $\Delta\boldsymbol{U}$ and $\boldsymbol{Y}$ is:

$$\boldsymbol{Y} = \boldsymbol{F}\boldsymbol{x}(k) + \boldsymbol{\Phi}\Delta\boldsymbol{U}, \tag{19}$$

where

$$\boldsymbol{F} = \begin{bmatrix} \boldsymbol{CA} \\ \vdots \\ \boldsymbol{CA}^{N_p} \end{bmatrix},$$

and

$$\boldsymbol{\Phi} = \begin{bmatrix} \boldsymbol{CB} & 0 & \cdots & 0 \\ \boldsymbol{CAB} & \boldsymbol{CB} & \cdots & 0 \\ \vdots & \ddots & \ddots & \vdots \\ \boldsymbol{CA}^{N_p-1}\boldsymbol{B} & \cdots & & \boldsymbol{CA}^{N_p-N_c}\boldsymbol{B} \end{bmatrix}.$$

The MPC strategy is designed to minimize both the depth control tracking error and the speed of response. These requirements are expressed as a quadratic cost function:

$$J = (\boldsymbol{R}_s - \boldsymbol{Y})^T(\boldsymbol{R}_s - \boldsymbol{Y}) + \Delta\boldsymbol{U}^T\boldsymbol{R}\Delta\boldsymbol{U}, \tag{20}$$

where vector $\boldsymbol{R}_s \in \mathrm{R}^{N_P\times1}$ is the reference depth sequence. In the second term, coefficient matrix $\boldsymbol{R} \in \mathrm{R}^{N_P\times N_P}$ is adjusted for the trade-off between tracking error and speed of response (control effort).

Substituting (19) into (20), the MPC depth control problem with hybrid actuation is described by the quadratic cost minimization problem:

$$\min J = \Delta\boldsymbol{U}^T(\boldsymbol{\Phi}^T\boldsymbol{\Phi} + \boldsymbol{R})\Delta\boldsymbol{U} - 2\Delta\boldsymbol{U}^T\boldsymbol{\Phi}^T(\boldsymbol{R}_s - \boldsymbol{F}\boldsymbol{x}(k)) \tag{21}$$

subject to the constraints:

$$\boldsymbol{x}(k+1) = \boldsymbol{A}\boldsymbol{x}(k) + \boldsymbol{B}\Delta\boldsymbol{u}(k)$$
$$x_3 \le u_v \le u_{max}$$
$$u_{min} \le u_p \le x_3$$
$$(u_v - x_3)(u_p - x_3) = 0.$$

There are two additional problems that must be solved to ensure the performance of the closed-loop system and reduce computational burdens: (a) selection of MPC parameters, and (b) the treatment of complementary constraints. These issues are addressed next.

3) MPC TUNING CONSIDERATIONS

MPC parameters N_p, N_c, and $\boldsymbol{R}$ are critical to system performance. The length of prediction horizon is N_p, which is the number of time steps to predict future output at each optimization iteration. Adjusting N_p affects the compromise between computational efficiency and prediction accuracy. Because the drifter system has significant nonlinearity,

behaviors over a long predictive horizon (large N_p) will deviate from the linearized operating point of the current iteration and may cause instability. On the other hand, a short prediction horizon cannot provide enough contributions for optimization. In general, 20-30 time steps have been found appropriate, given the low dynamics of the drifter.

Control horizon N_c ranges from 1 to N_p. Derivation of the matrices $\boldsymbol{F}$ and $\boldsymbol{\Phi}$ in (19) indicates that the tuning philosophy for N_c is similar to N_p, by balancing the computing resource and performance. This application takes advantage of the relatively slow dynamics of the submarine environment, and suggests that N_c be gradually increased to maximize the control performance.

Matrix $\boldsymbol{R}$ is a soft constraint on the rate of $\boldsymbol{u}$, and affects settling time and overshoot. This parameter is gradually increasted until the overshoot and settling time are acceptable.

4) COMPLEMENTARY CONSTRAINT PROCESSING

Equation (21) is subject to nonlinear inequality constraints. The problem can be converted to an unconstrained optimization problem by using the method of Lagrange multipliers, and then solved by Newton's method [26], but real-time implementation is difficult and solution accuracy cannot be guaranteed. In this work, the nonlinear constraints are treated as three different cases: $u_v = x_3$, $u_p = x_3$ and $u_v = u_p = x_3$. The corresponding control constraints are transformed as follows:

$$\begin{aligned} &a)\ u_v = x_3, \quad u_{min} \le u_p \le x_3 \\ &b)\ u_p = x_3, \quad x_3 \le u_v \le u_{max} \\ &c)\ u_v = x_3, \quad u_p = x_3, \end{aligned} \tag{22}$$

and u_c can be remapped to:

$$u_c = \begin{cases} u_p, & u_v = x_3 \\ u_v, & u_p = x_3 \\ u_p, & u_v = u_p = x_3. \end{cases} \tag{23}$$

Thus, MPC depth control of submarine drifter is expressed as an optimization problem to solve quadratic programming, where the nonlinearly constrained problem is equivalent to three linear quadratic programming problems. The three programming problems can be solved by the primal-dual method [27] and their optimal values can be found respectively in a few optimization iterations. The minimum optimal value among these case is the desired optimal value.

5) SOLVER IMPLEMENTATION

Algorithm (1) details the MCCMPC depth control algorithm of the drifter. The algorithm can be divided into three parts: real-time linearization, optimal value calculation, and state feedback. In each iteration, model (8) is linearized The optimal control sequence is obtained by solving the equivalent problem of complementary constraints. Finally, the latest control increment is output by the controller until the next iteration arrives.

Algorithm 1 MCCMPC Depth Control Algorithm of the Drifter

1: Initialize N_p, N_c, $\boldsymbol{R}$, r, maximum iteration k_{max}, $k = 1$, $u_c(0) = 0$;
2: **while** $(k \le k_{max})$ **do**
3: **Input** $\boldsymbol{x}^* = \boldsymbol{x}(k)$, $\boldsymbol{u}^* = \boldsymbol{u}(k-1)$;
4: Linearize $\dot{\boldsymbol{x}} = \boldsymbol{f}(\boldsymbol{x}, \boldsymbol{u})$ at $(\boldsymbol{x}^*, \boldsymbol{u}^*)$ to obtain $\boldsymbol{A}_c$ and $\boldsymbol{B}_c$;
5: Discretize model to obtain $\boldsymbol{A}$, $\boldsymbol{B}$, and $\boldsymbol{C}$.
6: Compute $\boldsymbol{\Phi}^T\boldsymbol{\Phi}$, $\boldsymbol{\Phi}^T\boldsymbol{R}_s$ and $\boldsymbol{\Phi}^T\boldsymbol{F}$;
7: Considering 3 cases:
$a)\ \min J_1 = J,\ s.t.\ u_v = x_3,\ u_{min} \le u_p \le x_3$
$b)\ \min J_2 = J,\ s.t.\ u_p = x_3,\ x_3 \le u_v \le u_{max}$;
$c)\ \min J_3 = J,\ s.t.\ u_v = x_3,\ u_p = x_3$
8: obtain $J_1(\Delta \boldsymbol{U}_1^*)$, $J_2(\Delta \boldsymbol{U}_2^*)$, $J_3(\Delta \boldsymbol{U}_3^*)$;
9: $\Delta \boldsymbol{U}^* = \arg\min\{J_1(\Delta \boldsymbol{U}_1^*),\ J_2(\Delta \boldsymbol{U}_2^*),\ J_3(\Delta \boldsymbol{U}_3^*)\}$;
10: Compute $\Delta \boldsymbol{U}^* = [\Delta \boldsymbol{u}(k), \Delta \boldsymbol{u}(k+1), \ldots, \Delta \boldsymbol{u}(k+N_c-1)]$;
11: $\boldsymbol{u}(k) = \boldsymbol{u}(k-1) + \Delta \boldsymbol{u}(k)$;
12: **Output** $\boldsymbol{u}(k)$;
13: $k = k + 1$;
14: **end while**

C. OTHER CONTROL METHODS FOR COMPARISON

PID control is one of two other control approaches that are considered. There exist well-established PID tuning methods that can treat the process as a "black box" to achieve desired performance [28]. For this application, the PID control approach fails to achieve the desired objectives. The hybrid actuator system switching behaviors and highly nonlinear system dynamics are not adequately considered by PID tuning.

The second control approach considered is the use of the disturbance observer, which treats the nonlinearity and anisotropy of the drifter as internal lumped disturbances, and estimates and compensates these disturbances [29], [30]. Under the framework of the disturbance observer, the drifter model can be rewritten as:

$$\dot{\boldsymbol{x}} = \boldsymbol{f}(\boldsymbol{x}) + \boldsymbol{g}_1(\boldsymbol{x})u_c + \boldsymbol{g}_2(\boldsymbol{x})\delta, \tag{24}$$

where $\boldsymbol{f}(\boldsymbol{x}) + \boldsymbol{g}_1(\boldsymbol{x})u_c$ represents the approximate characteristics of the drifter in one direction (either ascent or descent), while the other direction and the remaining uncertainties are expressed in disturbance term δ. Vector fields $\boldsymbol{g}_1(x), \boldsymbol{g}_2(x)$ are smooth with respect to $\boldsymbol{x}$, but (8) has nonlinear terms with sgn and max functions coupled to each other, and this will make the disturbance term have a more complex structure and stronger nonlinearity.

Performances of the proposed modified complementary constrained MPC (MCCMPC), conventional MPC, PID control, and disturbance observer based control (DOBC) are compared in the next section.

IV. VALIDATION

Experiments and simulations to validate the submarine drifter system are presented here. To guarantee the feasibility of the

proposed method, the model parameters of the drifter are firstly characterized by experiments. Simulation comparisons of several control methods are evaluated using M ATLAB S IMULINK.

A. IDENTIFICATION OF MODEL PARAMETERS

The overall dimension of the drifter is 0.8 × 0.8 × 3.0 m and contains four water sails arranged in a cross, an antenna, a set of linearly arranged sensors and an outer oil bladder. In the cabin of the drifter, there is a 24V battery, a STM32Fx microcontroller, a gear pump, a solenoid valve, an inner oil bladder and several sensors such as flow sensor, pressure sensor, etc.

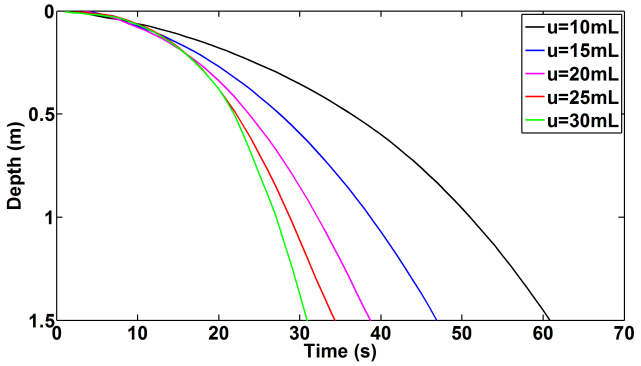

FIGURE 6. Response of the drifter to constant actuator outputs.

The drifter's parameters can be identified separately. For example, experiments of identifying the water damping coefficient k are carried out with five fixed actuator output values u. The real response are plotted in Fig. 6, and we can calculate k by fitting these curves according to equation (1). Buoyancy conversion coefficient k_{uF} can be obtained by calibrating the volume change of outer oil bladder caused by u. Pump's flow rate coefficient k_p and pressure-flow conversion coefficient k_{pq} can be measured by flow experiments. And the other parameters such as atmospheric pressure p_{atmos}, inner oil bladder pressure p_{in} and the depth-pressure conversion coefficient k_{dp} are known constants. The final state-space model of (15) is identified as:

$$\begin{bmatrix} \dot{x}_1 \\ \dot{x}_2 \\ \dot{x}_3 \end{bmatrix} = \begin{bmatrix} x_2 \\ (0.0084x_3 - 30{x_2}^2 \cdot S(x_2))/20 \\ 7.72\sqrt{0.0098066x_1 + 0.0213} \cdot S(u_v - x_3) \\ -8.23 \cdot S(x_3 - u_p) \end{bmatrix} \quad (25)$$

and the control constraints are identified as:

$$\begin{aligned} x_3 \le u_v \le 460 \\ -460 \le u_p \le x_3 \\ (u_v - x_3)(u_p - x_3) = 0 \end{aligned} \quad (26)$$

B. SIMULATION CONFIGURATION AND MCCMPC PARAMETER TUNING

MATLAB R2014a is used to simulate and compare depth control using PID, disturbance observer based control (DOBC), conventional model predictive control (MPC), and the proposed MCCMPC. In Sec. III-A, two methods for conventional MPC were described – the simulation comparisons use the first method. All programs are running on the Intel i5-4200U CPU. The sampling rate is 1 Hz.

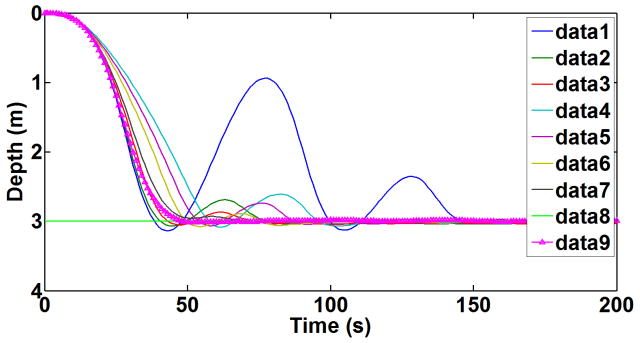

FIGURE 7. Parameter tuning of MCCMPC at $r = 3$m.

In Fig. 7, curves data1-data7 are the system responses during parameter tuning. The line data8 is the depth setpoint ($r = 3$m), and curve data9 is the satisfactory response achieved after tuning is completed.

At the start of tuning, the system is initialized with a small $\boldsymbol{R}$, a large prediction horizon N_p and a small control horizon N_c, resulting in large overshoot, as plotted in data1. Increasing $\boldsymbol{R}$ gradually reduces overshoot, as illustrated by data2 and data3. Tuning $\boldsymbol{R}$ is insufficient to achieve satisfactory performance; as discussed earlier, the prediction horizon N_p also affects response qualities. Curves data4 – data7 illustrate the effect of adjusting N_p. Control horizon N_c is gradually increased to achieve satisfactory system performance plotted in data9.

C. DEPTH CONTROL RESULTS

Two different depth set-point values of $r = 3$m and 10m are considered. For conventional MPC, the parameter ranges are $N_p \in [20, 30]$, $N_c \in [3, 10]$ and $R \in [0.2, 1]$, and the best performance is selected for comparison. The PID controller tuned by Ziegler-Nichols (ZN) method [31] resulted in controller gains $K_P = 2.3$, $K_I = 0.01$, $K_D = 10$, and the disturbance observer design follows the parameter tuning instructions in [32].

1) COMPARISON OF SETTLING TIMES

System response to PID control, disturbance observer based control (DOBC), conventional MPC, and the proposed MCCMPC are plotted in Figs. 8, 9, 10, and 11, respectively, for the dive from the surface to a depth $r = 3$m. It is important to note that the time scales are different for the four cases. There are clear differences in settling time; the drifter settles approximately 12 times faster under MCCPCC compared to PID control. The proposed MCCMPC response also settles faster than MPC and DOBC. Responses to a deeper dive ($r = 10$ m) are plotted in in Fig. 12, 13, 14, and 15. The proposed MCCMPC still takes the shortest time, about 65s.

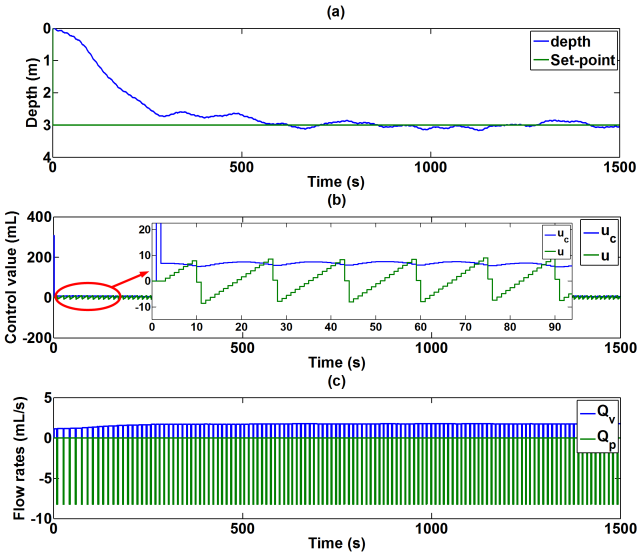

FIGURE 8. System response to PID control, $r = 3$m.

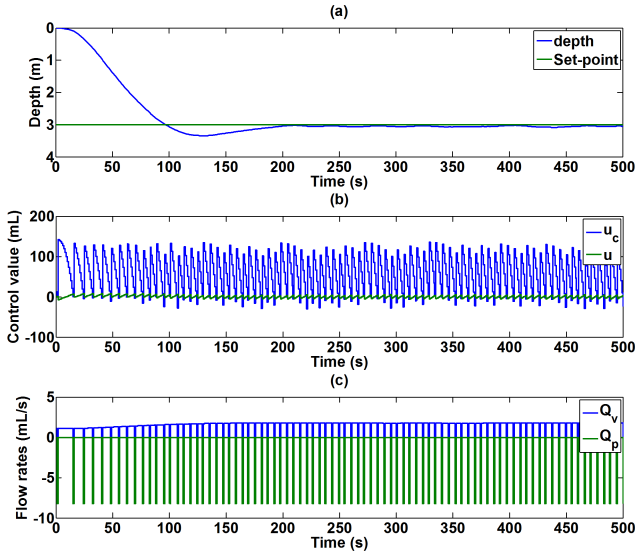

FIGURE 9. System response to DOBC, $r = 3$m.

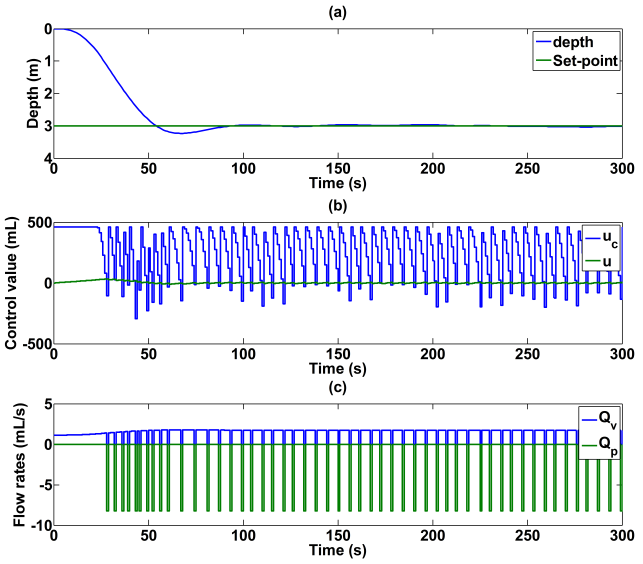

FIGURE 10. System response to MPC, $r = 3$m.

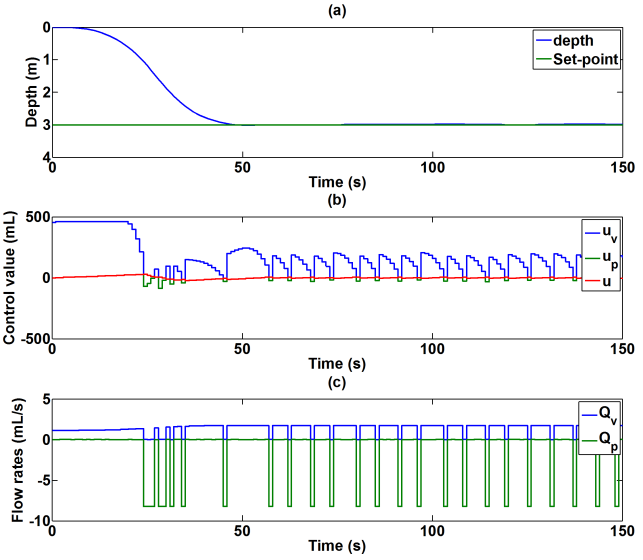

FIGURE 11. System response to proposed MCCMPC, $r = 3$m.

Responses to PID, DOBC and MPC take approximately 300s, 275s and 140s, respectively.

It may seem strange that the system response with PID control at larger set-point $r = 10$m is faster than the smaller set-point $r = 3$m. This strange phenomenon is determined by the interacting characteristics of both the PID controller and hybrid actuation system. Under PID control, a larger set-point value will produce a larger control output, which is beneficial to the diving acceleration process of the drifter. Furthermore, the solenoid valve flow rate gradually increases with diving depth.

2) COMPARISON OF STEADY STATE PERFORMANCE

Fig. 16 shows the comparison of errors among MCCMPC, MPC, PID and DOBC depth control at $r = 3$m and $r = 10$m. When the set-point is $r = 3$m, the drifter under PID control fluctuates about ± 0.15m, while it only fluctuates about ± 0.02m with MCCMPC. Although MPC and DOBC have significantly less fluctuations at the set-point than PID, they overshoot about 10% and 14%, respectively. When the set-point is $r = 10$m, the fluctuation of the drifter under PID control become worse and is about ± 0.2m with about 15% overshoot. MPC and DOBC also have 10% and 20% overshoot respectively. while the fluctuation of the drifter under MCCMPC is about ± 0.025m without any clear overshoots.

In summary, the MCCMPC approach can fully take advantage of modelling knowledge - it considers both the floating and the diving characteristics of the drifter, and achieves the best performance. The advantages will be discussed further in the following subsection.

TABLE 1. Rms error values and settling times for MCCMPC, PID, MPC and DOBC.

Setpoint (m)	RMSE[a]				Settling time (s)			
	MCCMPC	PID	MPC	DOBC	MCCMPC	PID	MPC	DOBC
1	0.0135	0.0597	0.0221	0.0262	45	639	82	181
2	0.0093	0.0766	0.0233	0.0258	47	620	87	193
3	0.0157	0.0785	0.0322	0.0292	50	598	90	200
4	0.0100	0.1186	0.0297	0.0311	52	552	96	209
5	0.0245	0.0649	0.0243	0.0221	55	501	104	223
6	0.0124	0.0713	0.0175	0.0325	57	459	111	231
7	0.0143	0.0525	0.0252	0.0312	59	393	118	243
8	0.0230	0.1244	0.0183	0.0271	61	351	125	258
9	0.0115	0.0984	0.0268	0.0298	63	322	132	266
10	0.0219	0.0998	0.0324	0.0301	65	301	140	275

[a]RMSE: Root Mean Squared Error.

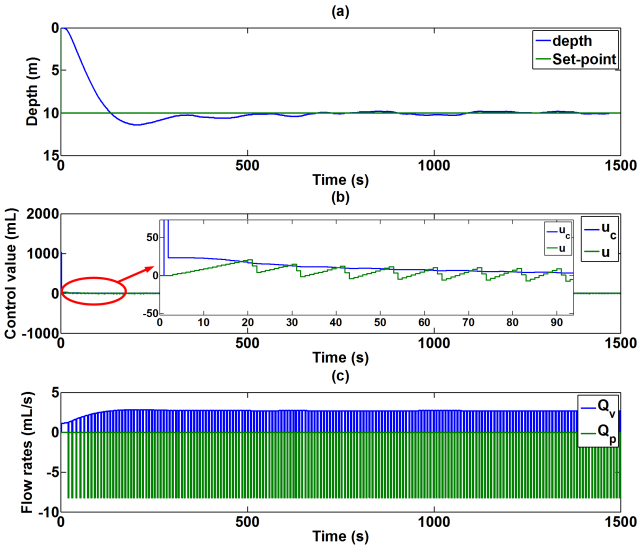

FIGURE 12. System response to PID control, $r = 10$m.

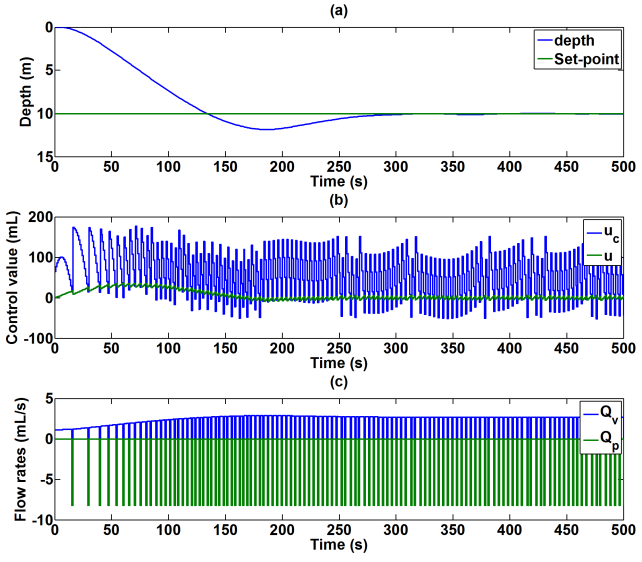

FIGURE 13. System response to DOBC, $r = 10$m.

3) ANALYSIS OF DEPTH CONTROL

We also simulate depth control from 1m to 10m in incremental steps of 1m. The rms error values and settling times are tabulated in Table 1.

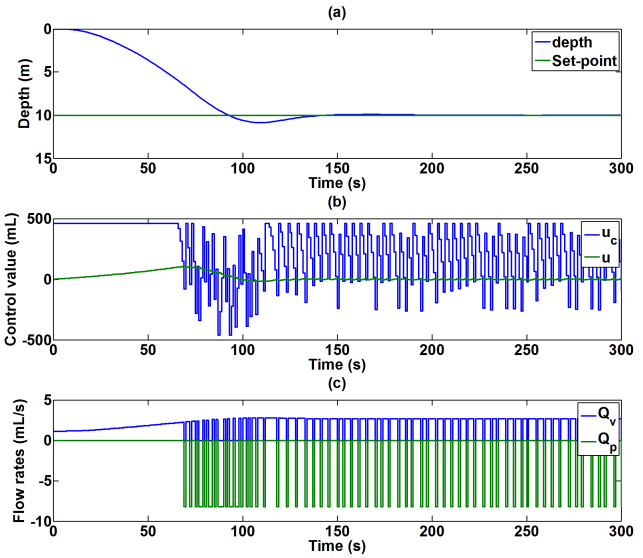

FIGURE 14. System response to MPC, $r = 10$m.

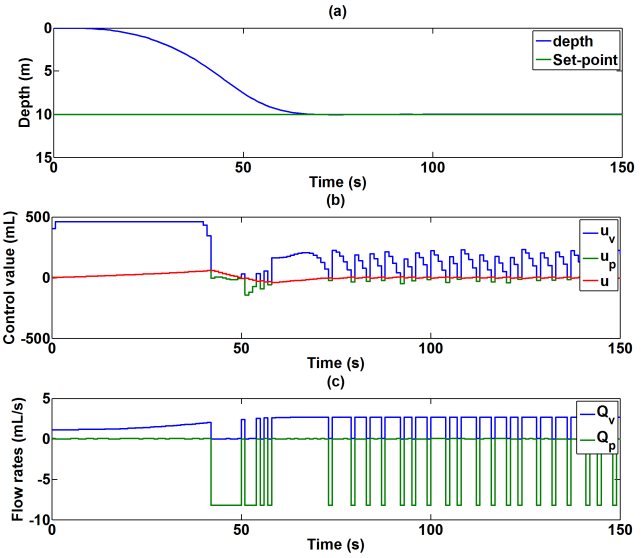

FIGURE 15. System response to proposed MCCMPC, $r = 10$m.

PID depth control has a overall worse performance than MCCMPC. It regards the drifter as a single-input single-output system, without considering the internal operating

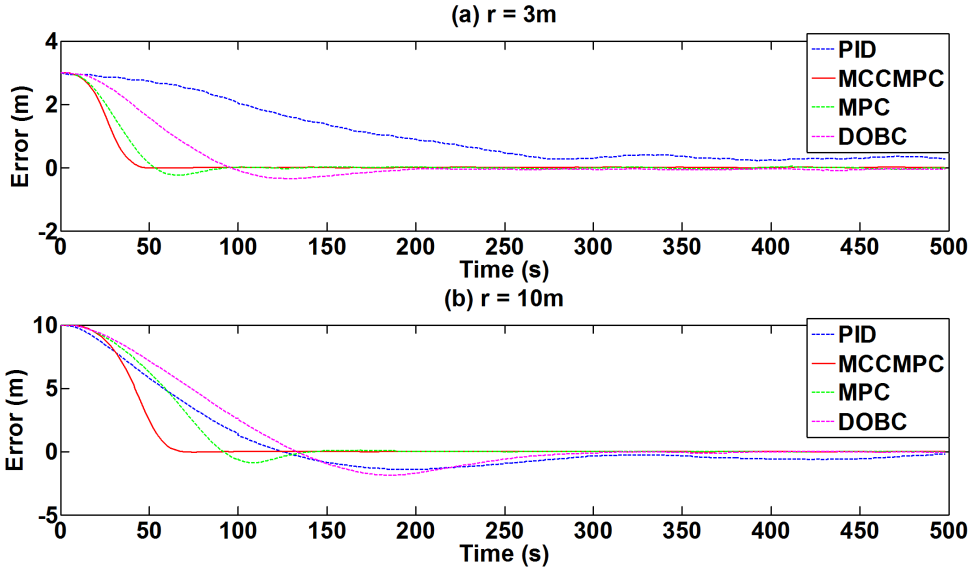

FIGURE 16. Comparison of error curves among PID, MCCMPC, MPC, and DOBC.

mechanism of the system. The magnified details of PID control in Fig. 8 and Fig. 12 show that the actuator has to switch between the pump and the valve in order to track u_c. At 1 Hz sampling frequency, the actuator output u will exceed or fall below the u_c within the sampling interval, which results in switching. As we can see from Fig. 8 and Fig. 12, although the drifter under PID control responds faster at $r = 10$m than $r = 3$m, the diving speed is not slowed down in advance which makes the drifter produce about 15% overshoot. The valve flow rate also increases nonlinearly with depth, while the pump flow rate remains constant. PID tuning does not account for these changes effectively, so the steady state performance under PID control cannot be guaranteed. Therefore, these defects of the PID controller cause the poor performances, which reflect in the slow system response and large fluctuation.

Compared with PID control, the performances of depth control using MPC and DOBC have been improved. However, they still show slower response speeds and large overshoots compared to MCCMPC. DOBC simplifies model (8) by considering the anisotropy and nonlinearity of the model as lumped disturbances, and uses disturbance observer to make compensation. Because the discontinuous functions such as sgn, max in the original model are coupled together, the disturbance term has a complex structure and strong nonlinearity. The disturbance observer cannot fully compensate it instantly, so the tracking speed of the drifter can be greatly affected. MPC makes prediction basing one direction's characteristic. When switching occurs between (9) and (10), the optimal solution and optimal state calculated by the previous submodel will not be applicable under the current submodel. Therefore, MPC that does not consider complementary constraints cannot achieve the desired control performance because of the large model mismatch.

In contrast, the MCCMPC solution has showed its merits from multiple aspects. The improvements are conducted by appropriately solving the nonlinear and non-ideal characteristics. It reformulates the SISO complex switch system into a two-input-single-output system with constraints which simplifies the controller design procedures. Then the flow characteristics between the pump and the valve are also taken into account based on the system model. With the well established nominal model, it predicts the future state within a certain time window based on the current state, and optimizes the controller output with cost function, which makes the switching between the pump and the valve more proactive. By reviewing the results that illustrated in Fig. 11 and Fig. 15, the results of the depth control with MCCMPC can be divided into three stages: dive accelerating, buffering and decelerating, and maintaining steady state. It makes predictions before the set-point arrives to slow down the drifter and proactively adjust the switching between the pump and the valve at the steady state, which makes the drifter respond quickly without overshoot and almost has no fluctuation at the set-point.

4) FEASIBILITY ANALYSIS OF MCCMPC ONLINE IMPLEMENTATION

The computation cost is the major concern for MPC-based controls. We evaluated the computation time of our proposed solver. In make a fair comparison, we also used MATLAB's nonlinear solver *fmincon* [33] to solve the complementary constraint in equation (21). That is, we use *fmincon* to directly obtain the optimal ΔU in Algorithm (1) instead of steps 7, 8, and 9. Fig. 17 shows the computational cost of Fig. 15.

After the equivalent constraints processing, the average time for the controller to calculate the optimal value in each

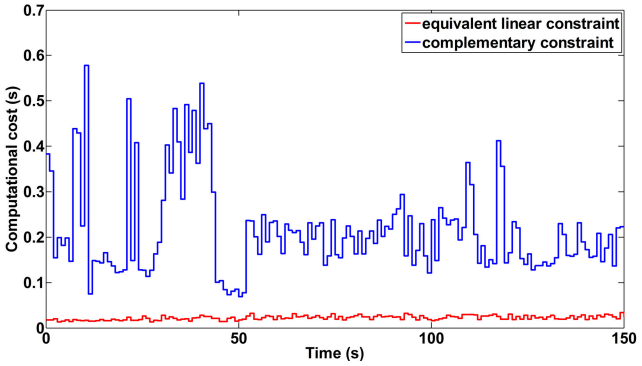

FIGURE 17. Comparison of computing burden between complementary constraint and equivalent constraint.

iteration only takes 0.02s, which is a small fraction of the 1s sample period. In contrast, it takes more than 10 times cost to solve the complementary constraints directly using *fmincon*. This is because we transformed the original nonlinear complementary constraint optimization problem into a linear constraint optimization problem. The solutions to the linear constrained optimization problems are all on the boundary of the convex polygon formed by its constraints, which is easy to find. Therefore, the processing of complementary constraint can satisfy the requirement of online MCCMPC implementation.

V. CONCLUSION

In this paper, a modified complementary constrained MPC scheme (MCCMPC) is proposed to precisely control the depth of a submarine drifter with hybrid actuation system, which cannot be processed efficiently by standard controllers. The drifter's control system model is established with equivalent constraints, and the model parameters of actual submarine drifter are characterized by experiments. The complementary constraint is transformed into three linear quadratic programming problems in order to implement online application. Compared with other three control methods, the proposed MCCMPC scheme achieves satisfied performance by solving the difficult nonlinear dynamics with complemenatary constraints and providing the accelerated optimization solver. The key metrics of the drifter under the proposed method show an overall improvement of 10x compared to classical methods.

We admit that this solution requires more works involving accurate system identification to conduct a reliable prediction model and relatively complex solver implementation. However, the validation sufficiently prove that this MCCMPC is able to fulfill the mission of depth control of the drifter. The suggested future work would be an auto tuning algorithm for MCCMPC and evaluate its anti-disturbance capability.

REFERENCES

[1] D. Roemmich, G. C. Johnson, S. Riser, R. Davis, J. Gilson, W. B. Owens, S. L. Garzoli, C. Schmid, and M. Ignaszewski, "The Argo Program: Observing the global ocean with profiling floats," *Oceanography*, vol. 22, no. 2, pp. 34–43, 2009.

[2] D.-H. Ji, H.-S. Choi, J.-I. Kang, H.-J. Cho, M.-G. Joo, and J.-H. Lee, "Design and control of hybrid underwater glider," *Adv. Mech. Eng.*, vol. 11, no. 5, 2019, Art. no. 1687814019848556.

[3] C. Pattiaratchi, T. University of Western Australia, L. M. Woo, P. Thomson, K. K. Hong, and D. Stanley, "Ocean glider observations around australia," *Oceanography*, vol. 30, no. 2, pp. 90–91, Jun. 2017.

[4] F. S. Tabataba'i-Nasab, A. Keymasi Khalaji, and S. A. A. Moosavian, "Adaptive nonlinear control of an autonomous underwater vehicle," *Trans. Inst. Meas. Control*, vol. 41, no. 11, pp. 3121–3131, Jul. 2019.

[5] B. A. Hodges and D. M. Fratantoni, "AUV observations of the diurnal surface layer in the North Atlantic salinity maximum," *J. Phys. Oceanogr.*, vol. 44, no. 6, pp. 1595–1604, Jun. 2014.

[6] R. Dehghani and E. Abedi, "An enhanced backstepping approach for motion control of underactuated autonomous surface vessels with input constraints," *Trans. Inst. Meas. Control*, vol. 40, no. 8, pp. 2669–2680, May 2018.

[7] I. Sakho, P. Dussouillez, D. Delanghe, B. Hanot, G. Raccasi, M. Tal, F. Sabatier, M. Provansal, and O. Radakovitch, "Suspended sediment flux at the rhone river mouth (France) based on ADCP measurements during flood events," *Environ. Monitor. Assessment*, vol. 191, no. 8, p. 508, Aug. 2019.

[8] S. Feng, R. T. Cheng, and X. Pangen, "On tide-induced lagrangian residual current and residual transport: 1. Lagrangian residual current," *Water Resour. Res.*, vol. 22, no. 12, pp. 1623–1634, Nov. 1986.

[9] R. Lumpkin, T. Özgökmen, and L. Centurioni, "Advances in the application of surface drifters," *Annu. Rev. Mar. Sci.*, vol. 9, no. 1, pp. 59–81, Jan. 2017.

[10] Z. Zhang, B. Qiu, P. Klein, and S. Travis, "The influence of geostrophic strain on oceanic ageostrophic motion and surface chlorophyll," *Nature Commun.*, vol. 10, no. 1, p. 2838, Dec. 2019.

[11] J. C. Ohlmann, M. J. Molemaker, B. Baschek, B. Holt, G. Marmorino, and G. Smith, "Drifter observations of submesoscale flow kinematics in the coastal ocean," *Geophys. Res. Lett.*, vol. 44, no. 1, pp. 330–337, Jan. 2017.

[12] M. S. Dortch, R. S. Chapman, and S. R. Abt, "Application of three-dimensional Lagrangian residual transport," *J. Hydraulic Eng.*, vol. 118, no. 6, pp. 831–848, 1992.

[13] Y. Chen, W. Jiang, X. Chen, T. Wang, and C. Bian, "Laboratory experiment on the 3D tide-induced lagrangian residual current using the PIV technique," *Ocean Dyn.*, vol. 67, no. 12, pp. 1567–1576, Dec. 2017.

[14] Y. Cui, W. Jiang, and F. Deng, "3D numerical computation of the tidally induced lagrangian residual current in an idealized bay," *Ocean Dyn.*, vol. 69, no. 3, pp. 283–300, Mar. 2019.

[15] C. Silvestre and A. Pascoal, "Depth control of the INFANTE AUV using gain-scheduled reduced order output feedback," *Control Eng. Pract.*, vol. 15, no. 7, pp. 883–895, Jul. 2007.

[16] H. Wu, S. Song, K. You, and C. Wu, "Depth control of model-free AUVs via reinforcement learning," *IEEE Trans. Syst., Man, Cybern. Syst.*, vol. 49, no. 12, pp. 2499–2510, Dec. 2019.

[17] M. Dong, J. Li, and W. Chou, "Depth control of ROV in nuclear power plant based on fuzzy PID and dynamics compensation," *Microsyst. Technol.*, vol. 26, no. 3, pp. 811–821, Mar. 2020.

[18] M. S. Mohd Aras, S. S. Abdullah, A. F. N. Abdul Rahman, N. Hasim, F. Abdul Azis, L. Wee Teck, and A. S. Mohd Nor, "Depth control of an underwater remotely operated vehicle using neural network predictive control," *Jurnal Teknologi*, vol. 74, no. 9, pp. 85–93, Jun. 2015.

[19] B. Li, Q. Hu, G. Ma, and Y. Yang, "Fault-tolerant attitude stabilization incorporating closed-loop control allocation under actuator failure," *IEEE Trans. Aerosp. Electron. Syst.*, vol. 55, no. 4, pp. 1989–2000, Aug. 2019.

[20] B. Li, Q. Hu, and Y. Yang, "Continuous finite-time extended state observer based fault tolerant control for attitude stabilization," *Aerosp. Sci. Technol.*, vol. 84, pp. 204–213, Jan. 2019.

[21] L. Wang, *Model Predictive Control System Design and Implementation Using MATLAB*. London, U.K.: Springer, 2009.

[22] D. Q. Mayne, J. B. Rawlings, C. V. Rao, and P. O. M. Scokaert, "Constrained model predictive control: Stability and optimality," *Automatica*, vol. 36, no. 6, pp. 789–814, Jun. 2000.

[23] J. Rossiter, *Model-Based Predictive Control: A Practical Approach*. Boca Raton, FL, USA: CRC Press, 2017.

[24] D. Mellinger and V. Kumar, "Minimum snap trajectory generation and control for quadrotors," in *Proc. IEEE Int. Conf. Robot. Autom.*, May 2011, pp. 2520–2525.

[25] S. Liu, N. Atanasov, K. Mohta, and V. Kumar, "Search-based motion planning for quadrotors using linear quadratic minimum time control," in *Proc. IEEE/RSJ Int. Conf. Intell. Robots Syst. (IROS)*, Sep. 2017, pp. 2872–2879.

[26] M. J. D. Powell, "Algorithms for nonlinear constraints that use lagrangian functions," *Math. Program.*, vol. 14, no. 1, pp. 224–248, Dec. 1978.
[27] D. Goldfarb and A. Idnani, "A numerically stable dual method for solving strictly convex quadratic programs," *Math. Program.*, vol. 27, no. 1, pp. 1–33, Sep. 1983.
[28] K. J. Aström and T. Hägglund, *PID Controllers: Theory, Design, Tuning*. Columbia, SC, USA: Scana, 1995.
[29] S. Li, J. Yang, W.-H. Chen, and X. Chen, *Disturbance Observer-Based Control: Methods and Applications*. Boca Raton, FL, USA: CRC Press, 2014.
[30] S. M. Shahruz, "Performance enhancement of a class of nonlinear systems by disturbance observers," *IEEE/ASME Trans. Mechatronics*, vol. 5, no. 3, pp. 319–323, Sep. 2000.
[31] K. J. Åström and T. Hägglund, "Revisiting the Ziegler–Nichols step response method for PID control," *J. Process Control*, vol. 14, NO. 6, pp. 635–650, 2004.
[32] E. Sariyildiz and K. Ohnishi, "Stability and robustness of Disturbance-Observer-Based motion control systems," *IEEE Trans. Ind. Electron.*, vol. 62, no. 1, pp. 414–422, Jan. 2015.
[33] M. Documentation, "Optimization toolbox, fmincon," MathWorks, Natick, MA, USA, Tech. Rep., 1999.

DALEI SONG received the Ph.D. degree from the Harbin Institute of Technology, Harbin, Heilongjiang, China, in 1999. He is currently a Professor with the Department of Automation and Measurement, Ocean University of China, Qingdao, China. His research interests include control systems, robotics technology, high-performance computing, machine learning, and artificial intelligence.

RENYU HOU received the B.E. degree from the College of Electrical and Automation Engineering, Shandong University of Science and Technology, Qingdao, China, in 2018. He is currently pursuing the master's degree with the College of Engineering, Ocean University of China, Qingdao. His research interests include underwater robot, model predictive control, and motion planning and optimization.

CHONG LI received the B.E. and M.E. degrees from the Ocean University of China, Qingdao, China, in 2009 and 2012, respectively, and the Ph.D. degree from Auburn University, Auburn, AL, USA, in 2016. He was a Postdoctoral Research Fellow with the Integrated MEMS Laboratory (IMEMS), Center for MEMS and Microsystems Technologies (CMMT), Georgia Tech, from 2016 to 2018. He is currently an Associate Professor with the Department of Automation and Measurement, Ocean University of China. His research interests include MEMS, control systems, high-performance computing, machine learning, and artificial intelligence.

JOHN Y. HUNG received the B.S. degree in electrical engineering from The University of Tennessee, Knoxville, TN, USA, in 1979, the M.S.E. degree in electrical engineering from Princeton University, Princeton, NJ, USA, in 1981, and the Ph.D. degree in electrical engineering from the University of Illinois at Urbana-Champaign, Champaign, IL, USA, in 1989. From 1981 to 1985, he was with Johnson Controls, Milwaukee, WI, USA, developing microprocessor-based controllers for commercial heating, ventilation, and air conditioning systems. From 1985 to 1989, he was a Consultant Engineer with Polyanalytics Inc. In 1989, he joined Auburn University, Auburn, AL, USA, where he is currently a Professor and the Graduate Program Coordinator with the Department of Electrical and Computer Engineering. He holds two U.S. patents in control systems. His teaching and research interests include nonlinear control systems and signal processing with applications in process control, robotics, electric machinery, and power electronics. He was the President of the IEEE Industrial Electronics Society, in 2014 and 2015, respectively. He received several awards for his teaching and research, including the Best Paper Awards from the IEEE TRANSACTIONS ON INDUSTRIAL ELECTRONICS and *IEEE Industrial Electronics Magazine*. He served as an Associate Editor for the IEEE TRANSACTIONS ON INDUSTRIAL ELECTRONICS, from 1996 to 2005, and the IEEE TRANSACTIONS ON CONTROL SYSTEMS TECHNOLOGY, in 1997 and 1998, respectively. He serves on the IEEE Board of Directors, in 2017 and 2018, respectively.

JILIANG WANG (Graduate Student Member, IEEE) received the B.S. degree from Shandong University, in 2014, and the M.S. degree in mechanical engineering from the Ocean University of China, in 2017. He is currently pursuing the Ph.D. degree in electrical engineering with Auburn University. His current research interests include neural networks, adaptive control, and robot control.